Journal of Applied Physics

Structural characterization of porous GaN distributed Bragg reflectors using x-ray diffraction

Cite as: J. Appl. Phys. **126**, 213109 (2019); https://doi.org/10.1063/1.5134143
Submitted: 30 October 2019 . Accepted: 21 November 2019 . Published Online: 04 December 2019

P. H. Griffin, M. Frentrup, T. Zhu, M. E. Vickers, and R. A. Oliver

Journal of Applied Physics ARTICLE scitation.org/journal/jap

Structural characterization of porous GaN distributed Bragg reflectors using x-ray diffraction

Cite as: J. Appl. Phys. **126**, 213109 (2019); doi: 10.1063/1.5134143
Submitted: 30 October 2019 · Accepted: 21 November 2019 ·
Published Online: 4 December 2019

View Online Export Citation CrossMark

P. H. Griffin,[a] M. Frentrup, T. Zhu, M. E. Vickers, and R. A. Oliver[a]

AFFILIATIONS

Department of Materials Sciences and Metallurgy, University of Cambridge, 27 Charles Babbage Road, Cambridge CB3 0FS, United Kingdom

[a]**Authors to whom correspondence should be addressed:** phg23@cam.ac.uk and rao28@cam.ac.uk

ABSTRACT

Porous GaN distributed Bragg reflectors (DBRs) provide strain-free, high-reflectivity structures with a wide range of applications across nitride optoelectronics. Structural characterization of porous DBRs is currently predominantly achieved by cross-sectional scanning electron microscopy (SEM), which is a destructive process that produces local data and has accuracy limited to around 3% by instrument calibration uncertainty. Here, we show that high-resolution x-ray diffraction (XRD) offers an alternative, nondestructive method for characterizing porous nitride structures. XRD scans of porous GaN DBRs show that despite the constant lattice parameter across the DBR layers, characteristic satellite peaks still arise, which are due to the interference between x-rays reflected from the porous and nonporous layers. By comparing the intensities and positions of the satellite peaks through diffraction patterns simulated from a kinematic model, the structural properties of the porous GaN DBRs can be analyzed. Using our method, we have measured a series of DBRs with stop bands from the blue wavelength region to the IR and compared their structural values with those from SEM data. Our results show that the XRD method offers improvements in the accuracy of determining layer thickness, although uncertainty for the value of porosity remains high. To verify the results gained from the XRD and SEM analysis, we modeled the optical reflectivity using the structural values of both methods. We found that the XRD method offered a better fit to the optical data. XRD, therefore, offers accurate, nondestructive characterization of porous DBR structures based on macroscale measurements and is suitable for full wafer analysis.

INTRODUCTION

Porous GaN distributed Bragg reflectors (DBRs) provide wavelength selective high-reflectivity structures, which can provide low strain, lattice-matched cavities required for GaN based vertical-cavity surface-emitting lasers (VCSELs),[1] as well as have wider applications across nitride optoelectronics.[2,3] The key advantage of porous DBRs, as compared to purely epitaxially grown ones, is that the alternating layers are perfectly lattice-matched and yet have a large refractive index contrast, which enables high reflectivity with low total thickness. These structures are produced via electrochemical etching after growth, which can be achieved through a single step process at the wafer-scale.[4]

Achieving the required reflectivity stop band, in terms of both the position and width, requires precise control of the thickness of the porous and nonporous layers, as well as the porosity of the porous layers. This demands characterization techniques that can accurately measure the structural properties of porous DBR structures. Previous works on porous GaN DBRs have used cross-sectional scanning electron microscopy (SEM) to characterize the structure.[5–8] This has the advantage of providing details on the morphology of the structure but has a number of limitations: it is a destructive process; it samples only small regions of the structure, which may not be representative; absolute thickness measurement is limited by an instrument calibration uncertainty of around 3%;[9] and obtaining an accurate value for the porosity is difficult, as it requires precise thresholding, which for highly porous structures remains a challenge.[10] Furthermore, SEM images are 2D projections of a 3D structure, and hence SEM is unable to measure the pore depth out of the plane of the image. Combining SEM imaging with focused ion beam (FIB) milling can allow thresholding techniques that use

the development of structures in the out of image plane,[11] but these methods increase cost and time significantly.

X-ray diffraction (XRD) might offer an alternative approach for structural characterization of porous DBR layers. It is nondestructive, fast, available at low cost, and is already well established for III-nitride heterostructures.[12] For example, Vickers *et al.* developed a method for the accurate determination of indium content and layer thicknesses in InGaN/GaN quantum well (QW) structures via XRD.[13] This was done by measuring a ω-2θ scan of the 0002 reflection, which showed periodic satellite peaks around the central GaN peak and a zero order peak separated from the GaN buffer layer peak. The satellite peaks were due to the periodic nature of the quantum wells (QWs), and the position of the zero order peak is given by the average In-content of the periodic structure. By fitting a model to the data, both the well width and indium content could be accurately determined. Vickers *et al.* describe how kinematic theory can be used to improve the understanding of how the structure relates to the diffraction data. Here, the solution is found by summing up the reflection from each atomic plane, while multiple scattering events are not included. This follows a mathematical step model as demonstrated previously.[14] In the case of porous GaN, XRD has previously been used to show that crystal quality is not degraded through porosification.[15] Here, we address an additional opportunity offered by XRD: structural characterization of porous GaN superlattices, such as DBRs. The key difference between a porous superlattice and a conventional one is that all the material has the same lattice parameters, meaning that there is no shift of the reciprocal lattice points and hence the position of the zero order peak cannot be used to determine an average porosity of periodic structure, as is similarly done for InGaN QWs. In this paper, we present a kinematic model capable of modeling periodic porous superlattice structures, such as DBRs. We demonstrate the method for fitting these results with measured XRD curves in order to characterize layer thickness and porosity of porous GaN DBRs. The findings were compared with results from conventional cross-sectional SEM measurements and used to model the reflectivity stop band for comparison with optical measurements.

METHODS

Material fabrication

Layers of gallium nitride were grown by metalorganic vapor-phase epitaxy (MOVPE) in a Thomas Swan close-coupled showerhead reactor[16] using trimethylgallium, ammonia, and silane as precursors on c-plane sapphire substrates. Periodic layers of nonintentionally doped (NID) GaN and Si doped n-GaN were created by modulating the silane flow. The n-GaN layers were then porosified following a single etch step process described elsewhere.[4] Three 10-pair DBR structures were grown with different layer thicknesses and a target doping density in the n-GaN layers of 10^{19} cm^{-3}. The three samples are referred to as A, B, and C and have target period thicknesses of around 95 nm, 110 nm, and 200 nm, respectively.

X-ray diffraction (XRD)

High-resolution x-ray diffraction measurements were performed on a Philips X'pert diffractometer with a 4-crystal Bartels primary monochromator ($\lambda = 1.540\,56$ Å) and an adjustable crossed slits collimator. The secondary beam optics consisted of a 3-crystal analyzer and a gas-proportional detector. All measurements were ω-2θ scans taken on the on-axis 0002 reflection or at low angles in the case of the x-ray reflectivity (XRR) data shown in the supplementary material.

Scanning electron microscopy (SEM)

Cross-sectional SEM data were collected from cleaved edges of the samples using both an FEI Nova NanoSEM and an FEI XL30 by imaging secondary electrons using the immersion lens in both cases.

Transfer matrix model (TMM)

A transfer matrix model (TMM) was used to simulate the optical reflectivity of a DBR structure, using an open source package for Python.[17,18] The model treats the structure as a series of individual layers with defined thickness and refractive index. The propagation of an electromagnetic wave through each layer is described by a matrix defined by the properties of the layer. The optical reflectance of a stack of layers can then be calculated using the product of these matrices. The TMM requires each layer to have a uniform refractive index. For a nonporous GaN layer, this is the refractive index of GaN, a function of wavelength that has been measured experimentally.[19] In the case of a porous layer, the effective refractive index can be calculated using the volume averaging theory[20] by

$$n = \sqrt{(1-\phi)\, n_{GaN}^2 + \phi\, n_{air}^2},$$

where ϕ is the porosity of the layer, while n_{GaN} and n_{air} are the refractive indices of GaN and air, respectively.

Optical reflectivity measurement

The optical reflectivity of DBRs was measured between 350 nm and 890 nm using an Ocean Optics experimental setup consisting of an Ocean Optics USB4000 spectrometer equipped with a fiber probe (Ocean Optics, R400-7-SR) and a dual deuterium and halogen light source (Ocean Optics DH-2000), using the halogen source only. A high-reflectivity reference standard was used to calibrate the setup (Ocean Optics, STAN-SSH).

XRD MODELING APPROACH

By using an appropriate model, structural values can be extracted from the XRD ω-2θ scan of a superlattice through fitting the simulation to the measured data. Modeling epitaxial nitride structures can be done with a variety of commercial software packages based on the dynamical approach, which has shown good agreement with experimental results.[13] This approach uses differential equations to solve the wave equation in the sample arising from a single scattering event. In the case of porous superlattices, this requires an accurate way of describing porosity within the model. The porous layers in the superlattice are a mixture of solid, crystallographic GaN and air, of which air has negligible scattering. This could feasibly be described by setting the occupancy of atom

positions in the crystal lattice to a value less than 1, in order to represent porosity. These calculations have been performed in commercial software giving similar results to our kinematic calculations. However, the former approach is awkward for fitting experimental data and using kinematic theory gives more details of the links between different aspects of the structure and the diffraction data. Moreover, for heteroepitaxial GaN strain is large and the density of defects is high, in which case a kinematic approach has been shown to be more appropriate.[13] Hence, we used a kinematic approach for our model, in which each layer is described by its thickness and the lattice parameter and scattering factor of the material. The scattering factor of the porous layers can, therefore, be described by the scattering factor of GaN multiplied by a site occupancy factor, which is given by the proportion of atoms left in the layer, i.e., $(1-\phi)$, where ϕ is the porosity.

In this work, a purpose-built kinematic model was created in MATLAB. This code is freely available, as detailed in the supplementary material. The porous GaN DBRs were defined in this model as periodic two-layer structures with five parameters:

1. Period thickness (γ)—the thickness of the repeating DBR pair (nm),
2. Thickness ratio (ρ)—the ratio between the thickness of the porous and nonporous layers,
3. Porosity (ϕ)—the volumetric proportion of the porous layer that is air (%),
4. Repeats (N)—the number of repeats of the periodic structure, and
5. Template thickness—the effective thickness of the GaN template (nm).

The first three of these parameters are the numbers that the model aims to obtain by comparing the simulated intensity profiles with experimental data. The number of repeats is known from the growth procedure. The appropriate value for template thickness is predominantly governed by scattering and absorption in the DBR layers.

The mathematics of the model follows the derivation previously set out by Vickers *et al.*[13] The model calculates the intensity by summing the scattering of each atomic plane in a DBR stack. This is described as

$$I = \frac{\sin^2(\pi\, k\, N\, \gamma)}{\sin^2(\pi\, k\, \gamma)} \left\{ \begin{array}{l} (1-\phi)^2 f_{GaN}^2 \dfrac{\sin^2(N_{Por}\, d_{GaN}\, \pi\, k)}{\sin^2(d_{GaN}\, \pi\, k)} + f_{GaN}^2 \dfrac{\sin^2(N_{NP}\, d_{GaN}\, \pi\, k)}{\sin^2(d_{GaN} \pi k)} + \\ 2\,(1-\phi)\, f_{GaN}^2 \cos(\pi k \gamma) \dfrac{\sin(N_{Por}\, d_{GaN}\, \pi\, k) \times \sin(N_{NP}\, d_{GaN}\, \pi\, k)}{\sin^2(d_{GaN}\, \pi\, k)} \end{array} \right\}, \tag{1}$$

where $k = 2\sin(\theta/\lambda)$, N is the number of porous layers, d_{GaN} is the atomic plane spacing of GaN, and f_{GaN} is its mean atomic scattering factor. The variable N_x gives the number of atomic planes for either the porous layer ($x =$ "Por") or the nonporous layers ($x =$ "NP"). The key difference between Eq. (1) and the previous work by Vickers *et al.* for InGaN/GaN quantum wells is that the plane spacing d_{GaN} is the same for both the porous and the nonporous layers. The thickness of each layer is given by $N_x d_{GaN}$, and ρ is simply the ratio between the thicknesses of the porous and the nonporous layers. Each term in Eq. (1) describes the contributions from the periodic structure, the porous layers, the nonporous layers, and the interference between the layers. It can, therefore, be simplified as

$$I = \Gamma[\alpha_{NP} + \alpha_{Por} + \alpha_{Inter}] = \Gamma\alpha, \tag{2}$$

where Γ is an interference term from the periodicity of the structure, α_{NP} and α_{Por} are the Bragg scattering terms due to the nonporous and porous layers, respectively, and α_{Inter} describes the scattering between these two layers.

Equations (1) and (2) form the core of our simulation procedure. In addition, the contribution from the GaN template below the DBR was simulated with a Gaussian function. Absorption was included, and this makes no significant difference to the intensities from the superlattice structure. Finally, to account for the finite resolution of the measurement system, the signal was convolved with a Gaussian representing the instrument function. As is common practice, the simulation was normalized to the zero order GaN reflection, which arises from a combination of the GaN substrate and the zero order peak of the superlattice.

An example for the simulated XRD intensity (and its components) of a periodic porous/nonporous DBR structure with 10 repeats is shown in Fig. 1(a). For this simulation around the 0002 GaN reflection, we have assumed a period thickness (γ) of 95 nm, a thickness ratio (ρ) of 0.4 between the porous and the nonporous layers, and a porosity (ϕ) of 30% in the porous layer. The central peak in the intensity profile I (top) corresponds to the 0002 GaN reflection, and around this, periodically spaced satellite peaks are visible. Examination of Fig. 1(a) shows that the locations of the satellite peaks are primarily defined by the peak positions of the interference term Γ, and are, therefore, dependent on the periodicity of the overall structure. The peaks of Γ are modulated by α, which behaves as an envelope function, defining the relative intensity of these peaks and shape of the overall curve. According to Eq. (2), α itself is the sum of its three components α_{NP}, α_{Por}, and α_{inter}. As one can see in Fig. 1(a), α_{Por} and α_{NP} are very similar with periodic troughs, but with a reduction in magnitude for the porous layer due to the scaling of the scattering factor by the porosity. The spacing of the troughs in α_{Por} and α_{NP} is defined by the individual layer thicknesses but can also be expressed in terms of multiples of the peak spacing in Γ. As in our example, the porous layer has a thickness of 2/5 of the period thickness (in real space), the spacing between troughs in reciprocal space is 5/2 times the spacing of the peaks in Γ. Similarly, the nonporous

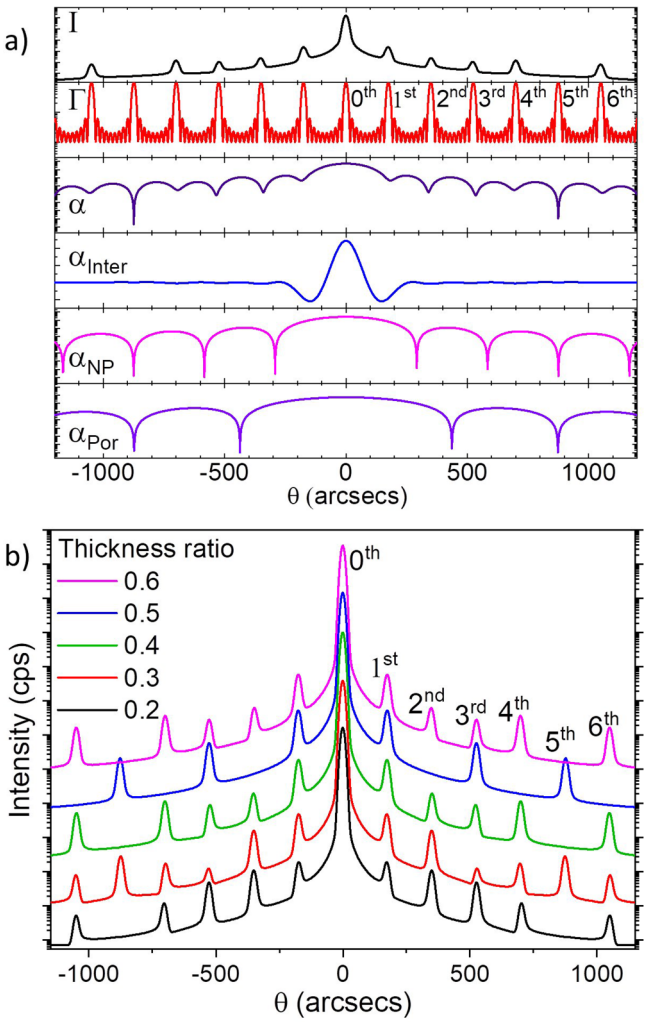

FIG. 1. Simulated ω/2θ scans of porous DBRs showing (a) the principal components of the simulation, as described in Eq. (2), for a DBR with 10 repeats, a period thickness of 95 nm, a thickness ratio of 0.4, and a porosity of 30%. All the curves are plotted on a log scale, except for α_{Inter}, which has negative regions and is plotted on a linear scale. (b) shows *I* for DBRs with varied layer thickness ratios, a constant period thickness of 95 nm, and a porosity of 30%. The curves have been offset from one another.

layer has 3/5 of the period thickness, and hence troughs can be observed in distances of 5/3 the peak distance in Γ from each other. A special case arises when the troughs of α_{Por} and α_{NP} align. This causes a deep trough in α, resulting in a missing satellite peak in the total intensity *I*. In our example in Fig. 1(a), this is the case at the 5th satellite peak in Γ, where the 2nd porous trough and the 3rd nonporous trough occur. This is the lowest common multiple of 5/2 and 5/3, the spacings between satellite peaks in the Γ function.

Figure 1(b) plots the simulated intensity profiles (I) for ω/2θ scans at the 0002 GaN reflection using the same model as in Fig. 1(a), but with a varied thickness ratio of the porous and nonporous layers (ρ) to illustrate how the position of the missing peaks shifts according to the description above. For better visualization, the curves were shifted vertically with respect to each other. In the case where the porous and nonporous layers are each half of the total period thickness (0.5), the spacing of the troughs in reciprocal space is double the satellite spacing, and hence every even numbered satellite peak is missing. The 5th peak is completely absent for the curves with thickness ratios 0.2, 0.4, and 0.6, where both layer thicknesses are some multiples of a 5th of the period thickness, as described above. It is not possible to distinguish between these cases based on the position of the missing peaks only. Instead, one also has to consider the relative intensities of the other satellite peaks. For example, the intensity profile for a thickness ratio of 0.2 can be distinguished from the other intensity curves by the relative intensities of the 1st and 4th satellite peaks, which are lower compared to the other curves. Lower intensity peaks like these can occur when one of the troughs in α_{NP} or α_{Por} partially overlaps a peak but does not perfectly align with it. Examples of this can be seen for the 2nd and 3rd peaks in Fig. 1(a). They can also occur when a deep trough lies near but not exactly on a satellite peak. This is the case for the 3rd satellite peak of the 0.3 ratio sample in Fig. 1(b). It can be seen to shift the peak position slightly, in this case reducing the intensity more severely on the small angle side and pulling the peak toward larger angles. These are more common in experimental samples, where the ratios are not such round numbers as have been simulated here.

It is important to note that if the thickness of the porous and nonporous layers is interchanged, such as for the simulations of the 0.4 and the 0.6 ratio, then the intensity curves show the same missing peaks and almost identical relative intensities of the other satellite peaks. These satellite peaks differ only slightly in magnitude due to the lower scattering factor of the porous layer, but this is likely to be insufficient to distinguish between the two cases from experimental data. The result of this is that fitting experimental data will generally lead to two solutions that are indistinguishable. It will not define which of the layers within a period is thicker. Hence, distinguishing between the two solutions requires knowledge from elsewhere, such as inputs from the chosen growth times for each layer. This approach may be challenging for structures where the layers have very similar thicknesses, as carrier diffusion from the doped layer may allow the electrochemical etching process to create pores in areas that were intended to be NID.

Figure 2(a) shows simulations with a constant period thickness γ of 95 nm, a thickness ratio ρ of 0.4, and varied porosity of the porous layer ϕ. Constant γ means that the Γ function remains the same, and hence the spacing between peaks does not change between these curves. In our examples, the 5th satellite peak is missing for all curves, which is defined by ρ as discussed above. The difference between the curves is in the overall intensity of the satellite peaks, which increases with increasing porosity. The highest relative intensities can be observed for the 100% porous "air-gap" DBR, while the 0% porous "unetched" DBR shows no satellite peaks at all. It should be noted that the 100% porous structure is included for theoretical interest only. Although air-gap DBRs have been created,[21] they are not physically realizable at the wafer-scale, nor at any scale that can be assessed by XRD, as the structure would collapse. The relative change in intensity across the satellite

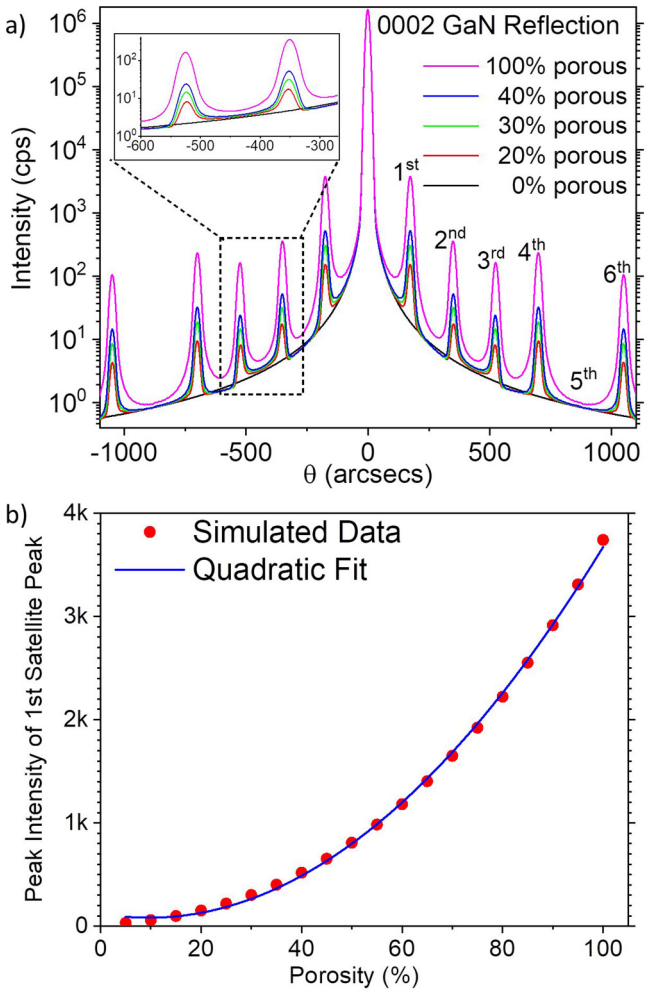

FIG. 2. (a) Simulated ω-2θ scans of porous DBRs for a 10 period DBR with a period thickness of 95 nm, a thickness ratio of 0.4, and varied porosity. (b) shows the peak intensity of the first satellite peak from these simulations as a function of the porosity in the porous layer.

peaks can be used to quantify the porosity of the porous layers of the DBR. Figure 2(b) plots the intensity of the 1st satellite peak with varied porosity for the data shown in Fig. 2(a). It indicates a quadratic relation between intensity and porosity. This follows from the quadratic relationship between the scattering factor and the total intensity in Eq. (1), as the scattering factor is proportional to the porosity of the layer. The examples discussed above show that the period thickness, thickness ratio, and porosity have different effects on the x-ray diffraction pattern. This allows decoupling of the effects and hence characterization of the DBR structure by fitting simulations to experimental XRD data.

RESULTS AND ANALYSIS

SEM results

Figure 3 shows cross-sectional SEM images of the three porous GaN DBR samples A, B, and C. Samples A and B have similar layer thicknesses and pore size, with pores that tend to occupy the whole width of the porous layer. Sample C has significantly thicker doped layers (and hence is shown at a lower magnification). This allows multiple rows of porosity to form in each layer. From these data, the period and layer thicknesses can be measured directly. Five SEM images with widths of 2.5 μm were analyzed for each sample, and an average and the standard error were calculated. Table I shows these results, with the error given as the larger of the 3% instrument calibration uncertainty and the standard error. The instrumental uncertainty is generally larger. These values are around the expected values from the growth times. For each sample, the porous and nonporous layers have similar thicknesses to one another. The period increases slightly from sample A to sample B and is much larger for sample C.

When analyzing SEM images, segmenting the image into porous and nonporous regions is a more challenging problem. Some regions of the porous layer show well defined pores that can be easily segmented [the solid box in Fig. 3(b)]. These are where the pores are relatively large and are aligned perpendicular to the image plane. In other regions, the pores are poorly defined, as they are smaller [the dotted box in Fig. 3(b)] or are aligned near to parallel with the image plane [the dashed box in Fig. 3(b)], which results in smooth edges that are difficult to segment and makes defining the actual volume of the pores very challenging. Cleaved

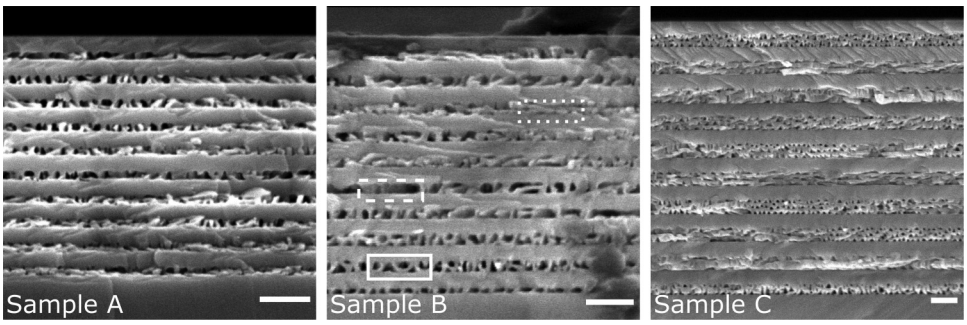

FIG. 3. Cross-sectional SEM images of three porous DBR samples: A, B, and C. Scale bars represent a width of 200 nm. Sample C has a period thickness around twice that of samples A and B. The three rectangles on sample B highlight regions with different pore morphologies: well defined, easily segmented pores (solid line), smaller, poorly defined pores (dotted line), and pores aligned along the image plane (dashed line).

TABLE I. Measured parameters of the DBRs from cross-sectional SEM.

	Period (nm)		Porous layer (nm)		Nonporous layer (nm)		Porosity (%)	
Sample	Value	±	Value	±	Value	±	Value	±
A	96	3	42	2	54	2	28	5
B	107	3	58	2	50	1	25	5
C	203	6	93	3	110	3	20	5

facets also often suffer from cleave lines and overhangs, which can cause image contrast in SEM data and make segmentation more challenging still. There are several approaches to image segmentation presented in the literature, but results tend to vary for different applications. We used segmentation techniques available with the Fiji distribution of analysis software ImageJ (version 1.52i) including local thresholding methods, such as the Phansalkar algorithm;[22] the level sets method, which uses the fast marching algorithm to find boundaries;[23,24] and the Weka segmentation algorithm,[25] which uses machine learning. Observations of the accuracy of these algorithms made it clear that for our data that the Weka segmentation algorithm was the best approach. However, it appeared to give an underestimate of porosity, as explained in more detail in the supplementary material along with a description of how the algorithm was implemented. The method requires the definition of seed areas, which makes it reasonably labor intensive; hence, we ran the algorithm on only two of the 2.5 μm wide SEM images for each sample. The porosity values given by the method are shown in the last column of Table I. This discussion illustrates some of the challenges of accurate analysis of the SEM data and shows that the level of complexity will vary between samples, depending on the pore size and pore alignment.

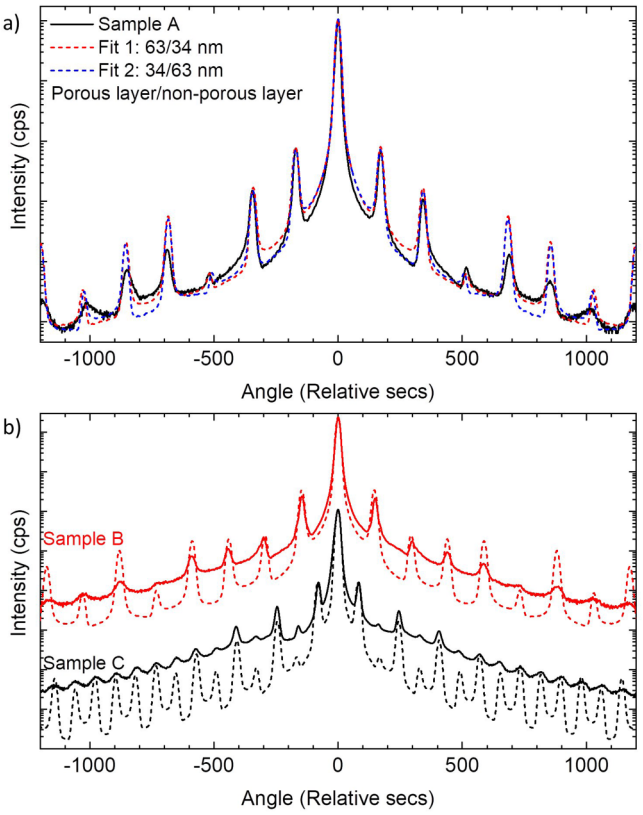

FIG. 4. ω/2θ scans of (a) sample A, showing the periodic satellite peaks with the two fitted simulations resulting from the two possible ρ values, and (b) samples B and C with the best fit simulation plotted as dashed lines.

XRD results

ω-2θ scans of the three samples A, B, and C were measured close to the 0002 GaN reflection. Figure 4(a) shows the XRD intensity profiles for sample A, which shows periodic satellite peaks around the GaN peak as predicted by the modeling. Obtaining the period thickness, ratio of the layer thicknesses in each period, and the porosity of the porous layer of the DBR is achieved by fitting our model to the measured data. As described previously, our model gives two possible solutions corresponding to two inverted values for ρ, i.e., if the fit gives $\rho = \rho_1$, then $\rho = 1 - \rho_1$ gives the second solution. The two plots obtained from the fitted simulation of sample A are shown alongside the measured data in Fig. 4(a), which shows that the difference between the two simulations is very small and neither gives a definitively better fit. This means that the XRD analysis gives two layer thicknesses, which cannot be assigned to the porous and nonporous layers without further input. For both plots, the period and shape of the envelope are well matched, but the absolute intensity of the higher order satellite peaks is not well matched. The model predicts less damping of the higher order peaks than is measured, and this is also seen in the measured and fitted plots for samples B and C, shown in Fig. 4(b). This indicates that there are nonidealities in the structure that are not represented in the model, such as the variation of layer thickness along or between the layers or the intrinsic roughness of porous layers. This difference between the model and the measurement leads to a large uncertainty in the extracted porosity value, as only the first few satellite peaks can be used to fit this parameter. Related work on porous silicon superlattices suggests that the damping might be due to graded interfaces between layers in the real DBR structure.[26] Fringes resulting from the total thickness of the structure may also arise, but these would have a spacing of less than the instrumental resolution and so are not measurable. The parameters extracted for each DBR by this method are shown in Table II.

A similar approach could be taken using low angle x-ray reflectivity (XRR), where similar oscillations have been used to extract structural information from InGaN/GaN quantum wells through simulation and fitting.[27] As this method is predominantly sensitive to the electron density, this could be well suited to characterizing porous materials, where the electron density varies strongly between porous and nonporous layers. Unfortunately, the characteristic peaks in these samples were smeared out and very poorly defined, which implies fluctuation of the layer thickness at a relatively long length-scale. This made

TABLE II. Measured parameters of the DBRs from XRD data.

	Period thickness (nm)		Porosity (%)		Layer thickness 1 (nm)		Layer thickness 2 (nm)	
Sample	Value	±	Value	±	Value	±	Value	±
A	97	1	37	4	34	1	64	2
B	113	1	54	10	47	1	66	1
C	205	1	44	10	97	1	108	1

fitting far more challenging than for the XRD method, as shown in the supplementary material.

Evaluating the two methods

Figure 5 shows the extracted thickness parameters for the DBR structures from the XRD and SEM techniques described above. The values for period thickness show reasonable agreement between all the methods, as plotted in the top plot of Fig. 5. The SEM values have larger error bars, due to the 3% calibration accuracy of the SEM and generally give slightly smaller values than the XRD approach. The middle plot of Fig. 5 shows the determined thickness of the individual layers in each period for the two methods. There is much more variation between these measurements, even when the period thicknesses estimates agree closely, such as for sample A. The bottom plot of Fig. 5 shows the extracted values for porosity from the Weka algorithm applied on SEM data and the fitted value from the XRD data using our model. Both these values have very large uncertainty, and they do not show the same trend. The error bars on the Weka values are due to the range in threshold value, as explained in the supplementary material. There is also uncertainty due to imperfect segmentation of the SEM data into pores and solid GaN. As discussed earlier, this is expected to lead to an underestimate of the porosity, which is demonstrated relative to the porosity derived by XRD in the bottom plot of Fig. 5. However, the porosity estimated by XRD itself has large uncertainty due to the poor fit of the model at higher order satellite peaks.

Predicting optical behavior

Given the structural parameters of a DBR structure, it is possible to predict its optical reflectivity and compare them with optical measurements of the three samples. This has been done using a transfer matrix model (TMM) of the optical reflectivity[28] for the parameters obtained from both the SEM and XRD approaches above. Figure 6 presents these results for the three samples plotted with the measured optical reflectivity in black. The stop band of each structure shifts from blue to green to infrared for samples A, B, and C, respectively, following the trend of increasing period thickness. Samples A and B have a shoulder at the short wavelength end of the stop band. The measurement for sample C is limited by the equipment available, which had a wavelength limit of 890 nm. This means that only the short wavelength end of the stop band can be measured. The two simulations using the fit parameters

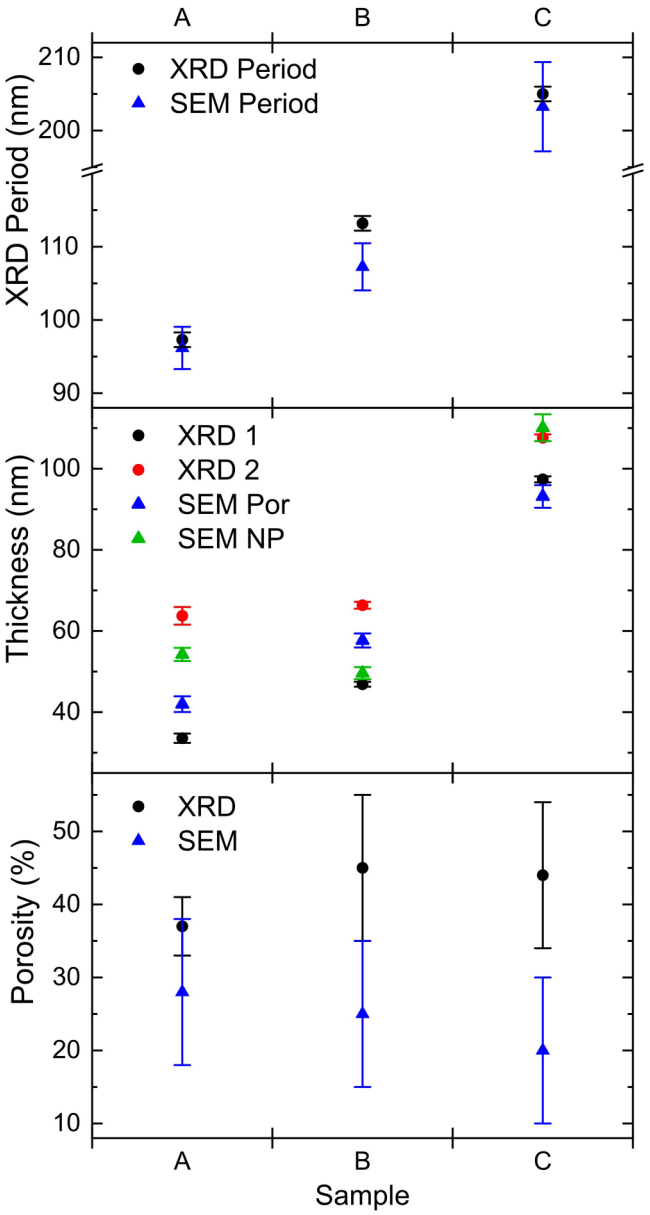

FIG. 5. Extracted data for the DBRs from XRD and SEM: (top) the period thickness of the structure, (middle) the individual layer thicknesses, and (bottom) the porosity of the porous layer.

from the XRD analysis are shown in red for the case that the nonporous layers are thicker (solid line) and thinner (dotted line) than the porous layers. Simulations using the SEM parameters are plotted in blue. The blue dotted line shows simulations, for which the thickness values from the SEM are combined with the porosity derived by XRD to allow a comparison of the difference in thickness values alone.

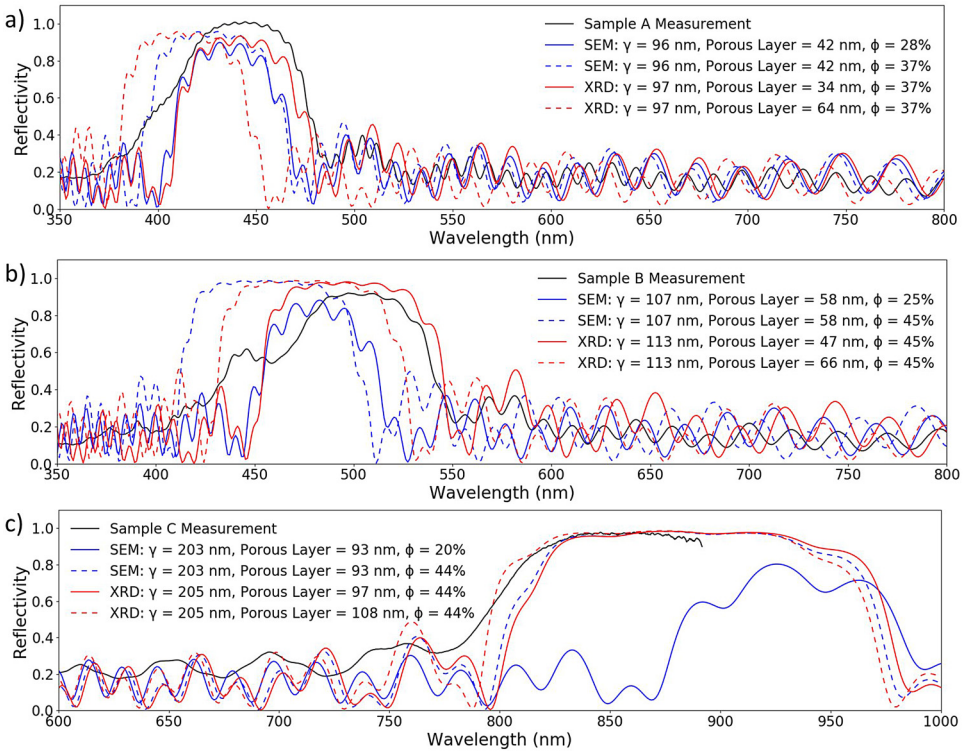

FIG. 6. Measured and TMM simulated reflectivity for the 3 DBR samples: A, B, and C. Each plot shows the measured optical reflectivity (solid, black) with TMM simulations using parameters from the SEM (blue, solid), SEM thickness parameters with the XRD porosity value (blue, dotted), and the two results of the XRD analysis for thicker solid layer (red, solid) and thicker porous layer (red, dotted).

In both samples A and B, the simulation based on XRD with a thicker nonporous layer agrees very well with the reflectivity measurements in terms of stop band location. The stop bandwidth is predicted fairly well for sample A but is too large in sample B, suggesting that porosity has been slightly overestimated by XRD. The simulations for samples A and B do not show the shoulders that these samples exhibit, but there are oscillations that are similar, although these oscillations are much lower in intensity and occur at a lower wavelength. This may be a sign of the disorder present in the real DBR, which also causes the oscillations to be less well defined than in the TMM simulations. Compared to this, both the stop bands simulated with the SEM results are shifted to lower wavelengths, due to the lower measured period thickness. The difference is even more apparent for the blue dotted curves, which used the layer thicknesses from the SEM analysis and the porosity derived from XRD by our model. The stop band width of the SEM-derived curves is also smaller, due to the lower porosity in the layers. For sample C, the thickness parameters of the two models agree very closely here, as for this larger structure, both methods—SEM and XRD—are reasonably good. The porosity measurement, however, differs considerably between the two methods, with the SEM approach yielding a significant underestimate. This is probably due to the larger area SEM image required to image the larger structure, which resulted in a lower resolution of the pores and making them harder to analyze. This could be compensated by increasing the image size when collecting the SEM data, but this will increase the acquisition time.

DISCUSSION

The comparison between the optical reflectivity of the three samples with simulated reflectivity spectra suggests that XRD may be preferred over SEM for measuring the thickness values of a porous DBR structure. Although both measurement approaches have a large uncertainty around the measurement of porosity, the optical data suggest that XRD measurements and simulations are more accurate and demonstrate better reliability than using SEM. With large, well-oriented pores, it is likely to be possible to achieve more accurate SEM measurements than are shown here within a tractable analysis methodology, but our results suggest that XRD is more robust to the analysis of a wide range of pore structures. XRD also has the advantage of giving an integrated measurement of the structure over an area of several square millimeters, whereas SEM is a highly localized measurement able to view a cross section of just tens of micrometers. SEM is also a destructive process, requiring the structure to be cleaved, and it is generally a more labor-intensive measurement.

CONCLUSIONS

We have demonstrated the use of high-resolution XRD to measure the structural parameters of porous GaN DBRs with reflectivity from blue to the IR. This is done by fitting the data to simulations obtained from a purpose-built kinematic model. Our results suggest that this approach yields more accurate measurements of layer thickness than analysis of SEM data. Measuring the porosity remains a challenge, as our method has high uncertainty

predicting this, requiring further development to our model to allow for nonidealities in the porous DBR layers. An x-ray based approach has the advantage over SEM of being nondestructive, less labor intensive, and giving a measurement that is representative over a large area.

SUPPLEMENTARY MATERIAL

Details of how to access the modeling code used in this project as well as experimental details of x-ray reflectivity measurements and the Weka image segmentation algorithm are given in the supplementary material.

ACKNOWLEDGMENTS

The authors would like to thank Dr. Fabrice Oehler (University Paris-Saclay) whose original code was used as the basis for developing our model. The authors would also like to acknowledge the Engineering and Physical Sciences Research Council (EPSRC) for financial support (Nos. EP/M010589/1 and EP/L015455/1) and the Impact Acceleration Account of the University of Cambridge (No. EP/R511675/1).

REFERENCES

[1]S. M. Mishkat-Ul-Masabih, A. A. Aragon, M. Monavarian, T. S. Luk, and D. F. Feezell, Appl. Phys. Express **12**, 036504 (2019).
[2]C.-J. Wu, G.-J. Wang, Z.-J. Yang, Y.-S. Lin, H. Chen, C.-H. Kao, J. Han, and C.-F. Lin, ACS Appl. Nano Mater. **2**(8), 5044–5048 (2019).
[3]G.-Y. Shiu, K.-T. Chen, F.-H. Fan, K.-P. Huang, W.-J. Hsu, J.-J. Dai, C.-F. Lai, and C.-F. Lin, Sci. Rep. **6**, 29138 (2016).
[4]T. Zhu, Y. Liu, T. Ding, W. Y. Fu, J. Jarman, C. X. Ren, R. V. Kumar, and R. A. Oliver, Sci. Rep. **7**, 45344 (2017).
[5]S. Mishkat-Ul-Masabih, T. S. Luk, A. Rishinaramangalam, M. Monavarian, M. Nami, and D. Feezell, Appl. Phys. Lett. **112**, 041109 (2018).
[6]J. Park, J.-H. Kang, and S.-W. Ryu, Appl. Phys. Express **6**, 072201 (2013).
[7]C. Zhang, S. H. Park, D. Chen, D.-W. Lin, W. Xiong, H.-C. Kuo, C.-F. Lin, H. Cao, and J. Han, ACS Photonics **2**, 980 (2015).
[8]P. Griffin, T. Zhu, and R. Oliver, Materials **11**, 1487 (2018).
[9]K. A. Bertness, NIST Special Publications SP 250-96, 2017.
[10]M. Salzer, S. Thiele, R. Zengerle, and V. Schmidt, Mater. Charact. **95**, 36 (2014).
[11]M. Salzer, T. Prill, A. Spettl, D. Jeulin, K. Schladitz, and V. Schmidt, J. Microsc. **257**, 23 (2015).
[12]M. A. Moram and M. E. Vickers, Rep. Prog. Phys. **72**, 036502 (2009).
[13]M. E. Vickers, M. J. Kappers, T. M. Smeeton, E. J. Thrush, J. S. Barnard, and C. J. Humphreys, J. Appl. Phys. **94**, 1565 (2003).
[14]A. Segmüller and A. E. Blakeslee, J. Appl. Crystallogr. **6**, 19 (1973).
[15]F. K. Yam, Z. Hassan, and S. S. Ng, Thin Solid Films **515**, 3469 (2007).
[16]R. P. Pawlowski, C. Theodoropoulos, A. G. Salinger, T. J. Mountziaris, H. K. Moffat, J. N. Shadid, and E. J. Thrush, J. Cryst. Growth **221**, 622 (2000).
[17]S. Byrnes, e-print arxiv.org/abs/1603.02720 (2016).
[18]S. Byrnes, Tmm: Simulate light propagation in multilayer thin and/or thick films using the Fresnel equations and transfer matrix method (2017).
[19]M. E. Lin, B. N. Sverdlov, S. Strite, H. Morkov, and A. E. Drakin, Electron. Lett. **29**, 1759 (1993).
[20]M. M. Braun and L. Pilon, Thin Solid Films **496**, 505 (2006).
[21]R. Sharma, Y.-S. Choi, C.-F. Wang, A. David, C. Weisbuch, S. Nakamura, and E. L. Hu, Appl. Phys. Lett. **91**, 211108 (2007).
[22]N. Phansalkar, S. More, A. Sabale, and M. Joshi, in *ICCSP 2011: International Conference on Communications and Signal Processing, Calicut, India, 10–12 February 2011* (IEEE, 2011), pp. 218–220.
[23]J. A. Sethian, Proc. Natl. Acad. Sci. U.S.A. **93**, 1591 (1996).
[24]E. Frise, J. Schindelin, A. Cardona, M. Hiner, and A.-M. Toersel, ImageJ segmentation plugins: Level sets, 2017, see https://imagej.net/Level_Sets.
[25]I. Arganda-Carreras, V. Kaynig, C. Rueden, K. W. Eliceiri, J. Schindelin, A. Cardona, and H. Sebastian Seung, Bioinformatics **33**, 2424 (2017).
[26]D. Buttard, D. Bellet, G. Dolino, and T. Baumbach, J. Appl. Phys. **83**, 5814 (1998).
[27]A. Krost, J. Bläsing, M. Lünenbürger, H. Protzmann, and M. Heuken, Appl. Phys. Lett. **75**, 689 (1999).
[28]C. C. Katsidis and D. I. Siapkas, Appl. Opt. **41**, 3978 (2002).